

Accepted Manuscript

Influence of Al content on the mechanical properties and thermal stability in protective and oxidation atmospheres of Zr-Cr-Al-N coatings

W.Z. Li, H.W. Liu, M. Evaristo, T. Polcar, A. Cavaleiro

PII: S0257-8972(13)00913-4
DOI: doi: [10.1016/j.surfcoat.2013.09.052](https://doi.org/10.1016/j.surfcoat.2013.09.052)
Reference: SCT 18901

To appear in: *Surface & Coatings Technology*

Received date: 30 May 2013
Accepted date: 30 September 2013



Please cite this article as: W.Z. Li, H.W. Liu, M. Evaristo, T. Polcar, A. Cavaleiro, Influence of Al content on the mechanical properties and thermal stability in protective and oxidation atmospheres of Zr-Cr-Al-N coatings, *Surface & Coatings Technology* (2013), doi: [10.1016/j.surfcoat.2013.09.052](https://doi.org/10.1016/j.surfcoat.2013.09.052)

This is a PDF file of an unedited manuscript that has been accepted for publication. As a service to our customers we are providing this early version of the manuscript. The manuscript will undergo copyediting, typesetting, and review of the resulting proof before it is published in its final form. Please note that during the production process errors may be discovered which could affect the content, and all legal disclaimers that apply to the journal pertain.

Influence of Al content on the mechanical properties and thermal stability in protective and oxidation atmospheres of Zr-Cr-Al-N coatings

W.Z. Li^{a, b, *}, H.W. Liu^a, M. Evaristo^b, T. Polcar^c, A. Cavaleiro^{b, *}

^a School of Materials Science and Engineering, Guangxi University, Nanning 530004, PR China

^b SEG-CEMUC - Department of Mechanical Engineering, University of Coimbra, Rua Luís Reis Santos, P-3030 788 Coimbra, Portugal

^c National Centre for Advanced Tribology at Southampton (nCATS), School of Engineering Sciences, University of Southampton, Highfield, Southampton, SO17 1BJ, Hampshire, UK

Corresponding author. Tel.: +351 239 790 745; fax: +351 239 790 701.

E-mail address: albano.cavaleiro@dem.uc.pt (A. Cavaleiro), wz-li@hotmail.com (W.Z. Li).

Abstract

Tools have been used under very high temperature in recent decades. Therefore, coatings on tools are required to be thermally stable and excellent in oxidation-resistance. The introduction of Al into nitride coatings was considered as an effective way to improve the coating oxidation-resistance and thermal stability. Quaternary Zr-Cr-Al-N coatings were deposited with increasing Al contents by d.c. reactive magnetron sputtering. The coatings were annealed at 800 and 900 °C for 1h in Ar + H₂ atmosphere and exposed at 700 °C for 2h and 1200 °C for 1h in air, respectively. The hardness, Young's modulus, adhesive/cohesive strength and residual stress of as-deposited and annealed coatings were characterized by nanoindentation, scratch test and curvature measurement method. The results showed that the coating hardness and Young's

modulus increased after post-annealing at 800 °C or 900 °C; the adhesive/cohesive strength decreased after annealing due to the substrate softening. The residual stress decreased after annealing and the lowest stress status depended on the crystallinity degree of the coating. XRD patterns showed mainly Cr₂O₃ formed in the Al-free, and a mixture of oxides of ZrO₂ and Al₂O₃ in the high Al coatings after 1200 °C/1h oxidation. N is still detected in the coatings, which indicates that the coatings are not fully oxidized being exposed to 700 °C for 2h.

Keywords: Zr-Cr-Al-N coatings; Mechanical properties; Thermal annealing; Oxidation; Microstructures

1. Introduction

In recent decades, Cr-N coatings have been widely investigated for cutting tools due to their excellent wear-resistance, anti-corrosion, and strong adhesion to the metallic substrates [1]. The optimization of the hardness of binary Cr-N coatings, by grain size refinement and/or residual stress effect, has not been high enough and, therefore, a third element has been often incorporated into the single nitride for achieving harder coatings [2]. Cr-Zr-N ternary coatings exhibit higher hardness compared to Cr-N ones due to a strong solid solution hardening promoted by the larger atomic radius of Zr in relation to Cr [3]. However, their lower onset oxidation temperature is a matter of worrying [4]. Kim et al. found that Cr-Zr-N coatings began to oxidize at 500 °C in air and their oxidation resistance further degraded with increasing Zr content [5].

Such a low onset oxidation temperature cannot fully satisfy the requirements of modern cutting tools. For high temperature coatings, Al plays an important role in the coating oxidation performance [6] being the oxidation resistance of the hard films strongly influenced by Al content [7-9]. It is reported that the onset oxidation temperature raised from 500 °C up to ~800 °C with

the addition of Al into CrN coatings [7]. On another study, the same value of 800 °C was observed in high Al Zr-Al-N coating [8]. Till now, there are only a few studies about effects of Al on the mechanical properties of quaternary Zr-Cr-Al-N coatings [10]. In a previous publication, we reported that a columnar structure was typical in Zr-Cr-Al-N coatings [10]. The hardness, Young's modulus, toughness and adhesive/cohesive strength of the coatings strongly depended on the Al content. Moreover, the coating mechanical properties were degraded for high Al contents. Nevertheless, the high temperature properties, including thermal stability and oxidation resistance, of Zr-Cr-Al-N coatings have not yet been studied requiring further investigation.

In this work, Zr-Cr-Al-N coatings with increasing Al contents were deposited by d.c. reactive magnetron sputtering. Thermal annealing tests in protective atmosphere and thermal exposure in air were performed. The influence of Al content on the structure, microstructure and mechanical properties of the as-deposited and annealed coatings was analyzed. Furthermore, the oxidation resistance of the coatings was evaluated.

2. Experimental Details

Quaternary Zr-Cr-Al-N coatings were deposited in a d.c. reactive magnetron sputtering system working in unbalanced mode. Pure Al, Cr and Zr targets (380 mm x 175 mm) were used; Al target was opposite to Zr target. The detailed configuration of the deposition system can be found elsewhere [10]. Different substrate materials were used for different measurement purposes: polished 100Cr6 steel coupons (25 mm in diameter) for mechanical properties measurement, stainless steel discs (25 mm in diameter and 0.5 mm in thickness) for residual stress analysis, polycrystalline alumina slices (dimensions 12 x 10 x 0.5 mm) for high temperature oxidation test and (111) silicon wafers for chemical composition and thickness evaluation.

After being ultrasonically cleaned in acetone for 15 minutes and alcohol for 15 min, the substrates were mounted in a substrate holder, which revolved around the center axis during deposition. Before deposition, the chamber was evacuated to less than 2×10^{-4} Pa and, then, Ar⁺ ion sputter-etching was used to remove any surface contaminants under a bias voltage of - 400 V for 20 min. For enhancing the interfacial adhesion of the subsequently deposited nitrided coating, a Cr adhesive interlayer, about 200 nm in thickness, was first deposited. The Zr-Cr-Al-N coatings were deposited in a mixed gas flow of 35 sccm Ar and 48 sccm N₂, under - 70 V substrate bias voltage for 180 min, with fixed power densities for Cr and Zr target set as 2.3 and 6.0 W/cm² respectively. Al target power densities were 0, 0.8, 1.5, 2.3 or 3.0 W/cm². After deposition, thermal annealing tests were conducted on the coating samples at 800 and 900 °C for 1 h in Ar + H₂ atmosphere. Thermogravimetric analysis was performed by exposing the samples to industrial air (99.995% purity) in a thermogravimetric analysis equipment (Setsys evolution 1750) where the temperature was increased from room temperature up to 1200 °C with a heating rate of 10 °C/min and then holding the samples at 1200 °C for 1 hour. High temperature oxidation-resistance tests were carried out at 700 °C for 2h by putting the coating samples in alumina crucible in the tube furnace.

The chemical composition of the coating was determined by energy dispersive X-ray (EDX) analysis. The thickness was obtained by profilometry. The phase structure was determined by X-ray diffraction (XRD) with Co K α radiation ($\lambda = 0.178897$ nm) in grazing mode (2°). The surface morphology of the samples was observed in a Carl Zeiss Optical Microscope (OM) and a scanning electron microscope (SEM), respectively. Transmission electron microscopy (TEM) experiments were carried out on a microscope JEOL-2200FS working at 200 KV. The

cross-section of the coating samples was prepared by tripod thinning method followed by precise ion milling technique.

The hardness (H) and Young's modulus (E) of the coatings, before and after thermal annealing, were measured by the Oliver and Pharr method [11]. The measurements were performed using a nanoindenter (Micro Materials NanoTest) with a diamond Berkovich tip at 10 mN applied load. The indentation depth was always less than 10% of the coating thickness [10]. For each sample, 12 measurements were performed. The adhesion/cohesion of the as-deposited and annealed samples was evaluated by scratch testing. The load was increased linearly from 0 N to ~70 N using a Rockwell C indenter with a 200 μm tip radius, a loading speed of 100 N/min and a scratch speed of 10 mm/min. The different failure modes were analyzed from the scratch tracks by optical microscopy.

The residual stresses in the as-deposited and annealed coatings were determined by Stoney's equation [12], being the curvature radii measured with an SP4 surface topography analyzer. During the measurement, only the central part of the sample was considered (17.5 mm length). In each sample, the curvature radii of horizontal and vertical directions were measured respectively and, in both directions, two profile scans were taken at two parallel lines separated by ~1 mm. The curvature radius value was averaged from these 4 measurements on the same sample. The detailed measurement process can be found in reference [13].

3. Results and discussion

3.1 Coating characterization

Table 1 shows the chemical composition and thickness of the coatings deposited with an increasing Al target power density. For simplicity, a designated name for each coating from its

chemical composition is given. From the chemical composition, it is clearly seen that Al content increases whereas Cr and N decrease with increasing Al target power density. The coating thickness is lower in the Al-free and ZrCrAl₃N coatings, then experiences a sudden increase when Al content is raised to 6 at.% or more, which is a result of the improvement of sputtering rate as the target working mode changes from “compound” to “metallic” [10]. As a consequence of the increase in the amount of sputtered target metallic atoms lower N content is reacted and the N/(Al+Zr+Cr) ratio decreased in the coating.

A typical columnar structure is observed in the ZrCrAl₃N coating from the bright field (BF) TEM cross-section images, as enhanced by the dot lines marked in Fig.1 (a). The SAD patterns revealed the diffraction planes from a single cubic phase. The diffraction rings can be assigned to (111), (200) and (220) planes corresponding to Cr(Zr,Al)N phase. From the high-resolution TEM (HRTEM) image in Fig.1 (b), a polycrystalline structure is shown for the coating. The Moiré fringes were caused by overlapping of sub-grains. The Fast Fourier Transformation (FFT) pattern in attached B demonstrates the single-crystal characteristics of the selected zone. The measured d spacing of the lattice fringes is 0.218nm, which is in between 0.207 nm of CrN (200) plane (JCPDS 11-0065) and 0.229 nm of ZrN (200) plane (JCPDS 35-0753).

The XRD results of the as-deposited and annealed coatings are shown in Fig.2. For the Al-free coating and low Al coatings (ZrCrAl₃N and ZrCrAl₆N), in both deposited and 800 °C annealed states, fcc B1 (NaCl type) phases were detected, whose diffraction peaks are located in between the positions of CrN and ZrN phases (Fig. 2(a, b)). This is consistent with the TEM results. After 800 °C annealing, the low crystalline structure was kept in the ZrCrAl₂₂N coating, and ZrN phase was detected in the ZrCrAl₂₇N coating. For 900 °C annealed samples, the precipitation of Cr

became apparent in the high Al coatings (ZrCrAl₂₂N and ZrCrAl₂₇N). The higher affinity of Zr for N than that of Cr [14] is in the origin of the precipitation of metallic Cr as a single phase. In fact, as the N content in these coatings is very low it will be combined preferentially with Zr. The excess of metallic elements in relation to the N available will favor the formation of metallic phases during the structural re-arrangement promoted by the thermal annealing. On the other hand, the cubic structure was retained in low Al coatings (Fig. 2 (c)). No wurtzite AlN phase was detected in the annealed coatings, which has been often reported to precipitate during thermal annealing in high Al content nitride coatings [1, 15]. Careful observation reveals that the shift of diffraction peaks is different between low and high Al coatings after thermal annealing. For instance, (111) peak central position is 41.26 ° and 40.34 ° for as-deposited ZrCrAl₆N and ZrCrAl₂₂N coatings, respectively, being shifted to 42.63 ° and 39.79 °, respectively, after 900 °C annealing. Therefore, peaks of annealed low Al coatings shifted to higher angles whereas those of high Al coatings shifted to lower angles close to the standard position of ZrN phase. In first case, the liberation of impurities entrapped in the crystal structure, including Ar, gives rise to a decrease of the lattice parameter. In the second case, the Cr precipitation from the fcc nitride structure leaves a more favorable ratio between Zr and N which, aided by the higher size of Zr atom in relation to Cr one, leads to higher interplanar distances after thermal annealing.

The presence of Zr oxides in some of the spectra after thermal annealing is due to the contamination by residual oxygen in the annealing atmosphere. As XRD was performed in glancing mode, the presence of thin oxide layers is enhanced.

The surface morphology of the annealed coatings was observed by optical microscope (not shown). After thermal annealing at 800 °C, the coating surface is rather smooth . However, when

annealing temperature was raised to 900 °C, wrinkling patterns could be found in ZrCrAl3N coating. EDS analysis showed that a little lower N content 42 at.% was detected in this annealed coating than in the as-deposited state. N content was also decreased to 38 at.% and 12 at.% in ZrCrN and ZrCrAl22N coatings respectively after 900 °C annealing .

3.2 Mechanical properties

The data of hardness, residual stress and Young's modulus as a function of the Al content, as well as their change after thermal annealing, are presented in Fig.3 (a, b, c). In order to evaluate the ability of the coating to resist cracking [16], H^3/E^{*2} ratio is calculated (H is the hardness, $E^* = E / (1-\nu^2)$ is the effective Young's modulus with Poisson's rate, $\nu = 0.25$) and the results are shown in Fig. 3 (d).

From Fig. 3(a), the hardness first increases and then decreases with the Al content in the coatings. Such a trend is related to the coating microstructural evolution, grain size refinement and solid solution effect [10]. Interestingly, a significant hardness enhancement is found in the 800 °C annealed coatings with low Al content, as compared to the as-deposited state, followed by a small decrease at 900 °C. It is often reported that the hardness increases in Ti-Al-N coatings after thermal annealing, due to the formation of coherent cubic domains, while phase segregation and stabilization of TiN and w-AlN occurs from the metastable single phase, which induce hardness decrease after further thermal treatment at higher temperatures [17]. In present system, the existence of a metastable cubic single-phase in the 800 °C annealed coatings was proved by XRD (Fig. 2). In other words, the decomposition did not take place (spinodal decomposition is not observed for CrAlN system [18]). However, if we consider atomic radii of Zr and Cr, it is possible that cubic ZrN phase precipitates at higher temperature; in such case the signature in XRD spectra

would be negligible. Small decrease in hardness when the annealing temperature was increased to 900 °C is not a result of the formation of wurtzite phase, since XRD spectra at both temperatures are almost identical. The presence of surface oxides is considered the main cause of such hardness decrease [19], although the impact of defects annihilation on the age hardening effect should not also be ignored.

The dependence of residual stress on the Al content and the thermal annealing temperature is shown in Fig. 3(b). As Al content increases, the residual stress in the as-deposited coatings first decreases, and then a little increase takes place when Al content is above 22 at.%. The variation of residual stress with the Al content is not only the result from the difference in coefficient of thermal expansion (CTE) between the coating and the substrate ($\alpha_{\text{CrN}}=2.3 \times 10^{-6} \text{ K}^{-1}$, $\alpha_{\text{ZrN}}=7.2 \times 10^{-6} \text{ K}^{-1}$, and $\alpha_{\text{steel}} \sim 12 \times 10^{-6} \text{ K}^{-1}$ [20]), but also from the different microstructural characterization. It is believed that a less compact columnar structure is beneficial to the stress relaxation for the high Al coatings. After thermal annealing, the residual stress experiences a significant decrease as compared to the as-deposited state. However, there is little detectable difference in the coating residual stress from the annealing temperature at 800 °C or 900 °C. It is known that thermal annealing is an effective way to relax the residual stress. During thermal annealing, diffusion of atoms is activated and then a rearrangement of atoms is induced. When thermal annealing is carried out on enough time, the atoms go into equilibrium state and defects are gradually annihilated, which remarkably decreases the internal stress in the coatings. Otherwise, the precipitation of solid solution can also reduce the dilatation of crystalline structure and thus to relax the coating stress. Due to low ratio of coating/substrate thicknesses in the present coating system [21], the effect of the coating thickness on residual stress is negligible.

The variation of Young's modulus with the Al content in the annealed coatings mostly follows the hardness variation (Fig. 3(c)), whereas two different points are present: first one is a marked decrease in the Young's modulus of the annealed Al-free coating compared to the as-deposited state, which should be the result from the formation of oxides during thermal annealing. The presence of surface oxides would impair the coating elasticity. Secondly, a higher Young's modulus is found in the 800 °C annealed high Al coatings than that of 900 °C annealing. From the observation of a very pronounced columnar structure with large column size in the high Al coatings [10], it is not impossible that thermal annealing treatment has densified the coating and therefore enhanced the Young's modulus. Herein, the effect of microstructural compactness on the modulus is stronger than that of surface oxides, and thus a higher modulus is detected in the 900 °C annealed high Al coatings.

From Fig. 3 (d), it is clear that the annealed coating exhibits an increase in the H^3/E^{*2} ratio as compared to the as-deposited one, indicating the improvement in the resistant of the coating to cracking or in the coating toughness after thermal annealing, which is commonly found in the annealed bulk metallic materials. In this work, the enhancement of H^3/E^{*2} ratio is related to the coating microstructural compactness, hardness increase and stress relaxation after thermal annealing.

Figure 4 shows the scratch tracks of the as-deposited and annealed coatings after scratching test. In the as-deposited state, Al-free coating, shows edge cracking at a load of 36 N being the substrate material exposed at 58 N (Fig. 4(a)). After 900 °C annealing, large area chipping takes place at only 20 N with full exposure of the substrate (Fig. 4(b)). A much better scratch test behavior was found when small amounts of Al are added to the coating. In the as-deposited

ZrCrAl₃N coating, cohesive failures are not pronounced, with appearance of conformal cracking at 42 N (Fig. 4(c)) followed by edge cracking for higher loads. No adhesive failures were observed up to the maximum test load. After annealing at 800 °C similar behavior could be registered, i.e. no adhesive failures and cohesive cracking starts to occur sporadically at load as low as 30 N (Fig. 4(d)). Full exposure of the substrate can only be detected for 64 N in the 900 °C annealed coating (Fig. 4(e)). In high Al content coatings, large area chipping is found at 48 N (Fig. 4(f)) in the as-deposited state, which is detected for much lower loads (16 N) in the annealed samples (Fig. 4(g)). The global worse critical loads behavior of annealed samples compared to as-deposited ones should be attributed to the softening of the substrate during thermal annealing. Considering the same applied load during the scratch testing, the plastic deformation of the substrate should be much higher in the annealed samples due to their lower yield strength. The coating will be submitted to a higher strain increasing the cracking probability. Therefore, for similar coating properties cracking and coating delamination should occur for lower applied loads, i.e. those leading to applied strain to the coatings similar to those in the as-deposited state for which those failures occur. Lin et al. reported similar results having observed that the same coating on soft steel substrate exhibited a lower critical load for coating failure than that on a hard one [22]. Finally it should be remarked that, taking into account the above results for the H^3/E^{*2} parameter, annealed coatings should exhibit increased toughness which would improve the coating adhesive/cohesive strength, factor which could compensate the referred effect of substrate softening.

3.3 Onset oxidation behavior

Figure 5 shows the TGA results of the coatings with different Al contents exposed to air till

1200 °C. All coatings start oxidization at about 600 °C, indicating that the addition of Cr can improve the oxidation resistance as compared to the binary ZrN coating, which exhibits an oxidation onset at ~500 °C [23, 24]. No significant differences are observed among the 3 studied coatings although the oxidation curve seems to be slightly steeper for the coatings with Al content. Al-free coating shows mass stabilization at a temperature close to 800 °C, suggesting that the coatings was mostly consumed and Al₂O₃ substrate is completely inert. The weight gain in ZrCrAl₂₂N coating was much higher than for the other two coatings which can be understood either by its much higher thickness (~ 4x higher) or its lower N content. During oxidation, N is liberated to atmosphere acting inversely in the weight gain, trend which should have less importance in this coating having lower N content. Unexpectedly, a marked loss in the mass gain is observed in this coating at ~1100 °C, which can be an outcome of the spallation of the surface oxides. Following to this zone, stabilization of the weight gain is observed, again suggesting the complete degradation of the coating. In Cr-N and Cr-Al-N coatings the onset oxidation temperature is close to 800 °C [7], while the temperature decreases to 600 °C for Zr-Cr-N coatings deposited with different Zr/Cr ratio [4]. This was also observed in the present work with the onset of oxidation at 600 °C, even in the coatings with Al addition. Only for very high Al contents when an Al-rich nitride phase was preferentially formed [8], Zr-Al-N films can show an improved oxidation resistance (onset at 800 °C). The oxidation products of the coatings after thermal exposure at 1200 °C were characterized by XRD and were observed by SEM, as shown in Fig.6. In Al-free and low Al coatings, mainly Cr₂O₃ and ZrO₂ was formed (Fig. 6(a)). The surface is rather rough with defects, such as holes and cracks (Fig. 6(b)). The cross-sectional BSE images show that the two coatings are fully oxidized (Fig. 6(c-e)). The m-ZrO₂ (monoclinic) phase

became dominating and no Cr_2O_3 was detected any more in the XRD results (Fig. 6(a)). The m- ZrO_2 phase should be transformed to tetragonal structure at the temperature above $\sim 1100^\circ\text{C}$ [24, 25] and reverse transformation during cooling down. However, the coexistence of m- and t- ZrO_2 was still found after 1200°C annealing. Franz et al [8] showed that the presence of Al can influence the m-to-t phase transformation, which can explain the higher relative amount of t-phase in the coating with the highest Al content.

Obviously the coatings are less protective when the exposure temperature is higher than $800\sim 900^\circ\text{C}$. The coating samples with Al addition were exposed to air at 700°C for 2h to investigate the oxidation resistance. Although surface oxidation was evident, EDS analysis indicated that N could be still detected in the coatings; N content was about 11 at.% and 14 at.% for the $\text{ZrCrAl}_{13}\text{N}$ and $\text{ZrCrAl}_{22}\text{N}$ coatings, respectively. Thus, the coatings were not fully oxidized at 700°C .

4. Conclusion

Quaternary Zr-Cr-Al-N coatings with the different Al contents were deposited by d.c. reactive magnetron sputtering. The coatings exhibited a columnar microstructure. The as-deposited Al-free and low Al coatings had an fcc NaCl-type B1 structure and the structure was still retained in the annealed states. The low crystalline degree in the high Al coatings were improved after 900°C thermal annealing, and slight oxidization was detected in the Al-free and high Al coatings.

The enhancement of hardness, Young's modulus and H^3/E^{*2} ratio, and the relaxation of residual stress were found in the annealed Al-contained coatings. The adhesive/cohesion strength was reduced in the Al-free and high Al coatings after thermal annealing. The combined effects of microstructural evolution, phase separation, oxides formation and substrate softening, etc were

responsible for the change of mechanical properties of the annealed coating systems.

The onset oxidation temperature was about 600 °C, which was strongly determined by the oxidation of Zr-rich nitride phase. With the increase of Al content in the coatings, the main oxidation products changed from Cr₂O₃ to ZrO₂ during exposure to 1200 °C. Oxides particles are formed and rather high N contents (~11 at.%) are still present in the coatings after being oxidized at 700 °C for 2h. The coatings are protective under such a temperature.

Acknowledgements

This work was supported by the Portuguese Foundation for Science and Technology (FCT, through SFRH/BPD/76925/2011 and PTDC/EME-TME/122116/2010 grants), and the National Natural Science Foundation of China (Grant Nos.51001032, 51371058 and 51371059) and China-Portugal bilateral project, Guangxi Science Foundation (Grant Nos. 0731013 and 2010GXNSFD013006), which are gratefully acknowledged. The authors are grateful to Nelson Santos Duarte and Jorge Corker from IPN at Coimbra for the XRD and TGA measurements, respectively.

References

- [1] P.H. Mayrhofer, C. Mitterer, L. Hultman, H. Clemens, *Prog. Mater. Sci.* 51 (2006) 1032.
- [2] C.S. Sandu, R. Sanjinés, M. Benkahoul, F. Medjani, F. Lévy, *Surf. Coat. Technol.* 201 (2006) 4083.
- [3] G.S. Kim, B.S. Kim, S.Y. Lee, J.H. Hahn, *Surf. Coat. Technol.* 200 (2005) 1669.
- [4] S.Y. Lee, Y.S. Kim, G.S. Kim, *J. Vac. Sci. Technol. A* 27 (2009) 867.
- [5] S.M. Kim, B.S. Kim, G.S. Kim, S.Y. Lee, B.Y. Lee, *Surf. Coat. Technol.* 202 (2008) 5521.
- [6] W.Z. Li, Y.Q. Li, C. Sun, Z.L. Hu, T.Q. Liang, W.Q. Lai, *J. Alloys Compd.* 506 (2010) 77.

- [7] J. Lin, B. Mishra, J.J. Moore, W.D. Sproul, Surf. Coat. Technol. 202 (2008) 3272.
- [8] R. Franz, M. Lechthaler, C. Polzer, C. Mitterer, Surf. Coat. Technol. 206(2012) 2337.
- [9] A. Hörling, L. Hultman, M. Odénb, J. Sjöln, L. Karlsson, Surf. Coat. Technol. 191 (2005) 384.
- [10] W.Z. Li, M. Evaristo, A. Cavaleiro, Surf. Coat. Technol. 206 (2012) 3764.
- [11] W.C. Oliver, G.M. Pharr, J. Mater. Res. 7 (1992) 1564.
- [12] G.G. Stoney, Proc. R. Soc. London Ser. A 82 (1909) 172.
- [13] A. Cavaleiro, A.P. Marques, J.V. Fernandes, N.J.M. Carvalho, J.Th. De Hosson, J. Mater. Res. 20 (2005) 1356.
- [14] I. Barin, Thermochemical Data of Pure Substances, Third Edition, VCH Verlagsgesellschaft mbH., Weinheim, 1995, p. 567, 1878.
- [15] M. Bartosik, R. Daniel, Z. Zhang, M. Deluca, W. Ecker, M. Stefenelli, M. Klaus, C. Genzel, C. Mitterer, J. Keckes, Surf. Coat. Technol. 206 (2012) 4502.
- [16] J. Musil, M. Jirout, Surf. Coat. Technol. 201 (2007) 5148.
- [17] P.H. Mayrhofer, A. Hörling, L.Karlsson, J.Sjöln, T.Larsson, C.Mitterer, L.Hultman, Appl. Phys. Lett. 83 (2003) 2049.
- [18] P.H. Mayrhofer, H. Willmann, L.Hultman, C.Mitterer, J. Phys. D: Appl. Phys. 41 (2008) 155316.
- [19] A. Flink, T. Larsson, J. Sjöln, L. Karlsson, L. Hultman, Surf. Coat. Technol. 200 (2005) 1535.
- [20] H. Holleck, J. Vac. Sci. Technol. A 4 (1986) 2661.
- [21] C. A. Kleina, J. Appl. Phys. 88 (2000) 5487.

[22] J. Lin, J.J. Moore, W.D. Sproul, B. Mishra, Z. Wu, J. Wang, *Surf. Coat. Technol.* 204 (2010)

2230.

[23] S. Luridiana, A. Miotello, *Thin Solid Films* 290–291 (1996) 289.

[24] G.L.N. Reddy, J.V. Ramana, S. Kumar, S.V. Kumar, V.S. Raju, *Appl. Surf. Sci.* 253 (2007)

7230.

[25] Y.K. Voronko, A.A. Sobol, V.E. Shukshin, *Phy. Solid State* 49 (2007) 1963.

ACCEPTED MANUSCRIPT

Figure captions

Fig.1 Cross-section BF-TEM (a) and typical HRTEM image (b) of the as-deposited ZrCrAl₃N coating. The corresponding SAD patterns are inserted in (a). The FFT spectra and IFFT image of the selected zone in (b) are attached in B and C, respectively.

Fig.2 XRD patterns of the coatings as-deposited (a), annealed at 800 °C (b) and 900 °C (c).

Fig.3. Hardness (a), residual stress (b), Young's modulus (c) and H^3/E^{*2} (d) of the as-deposited and annealed coatings.

Fig.4. Typical track morphologies of the ZrCrN (a, b), ZrCrAl₃N (c, d, e) and ZrCrAl₂₇N (f, g) coatings before and after annealing.

Fig.5. TGA curves of the ZrCrN, ZrCrAl₃N and ZrCrAl₂₂N coatings exposed to air from room temperature to 1200 °C.

Fig.6. XRD patterns (a) and SEM images of the ZrCrN (b, c), ZrCrAl₃N (d) and ZrCrAl₂₂N (e) coatings exposed to air at 1200 °C for 1h.

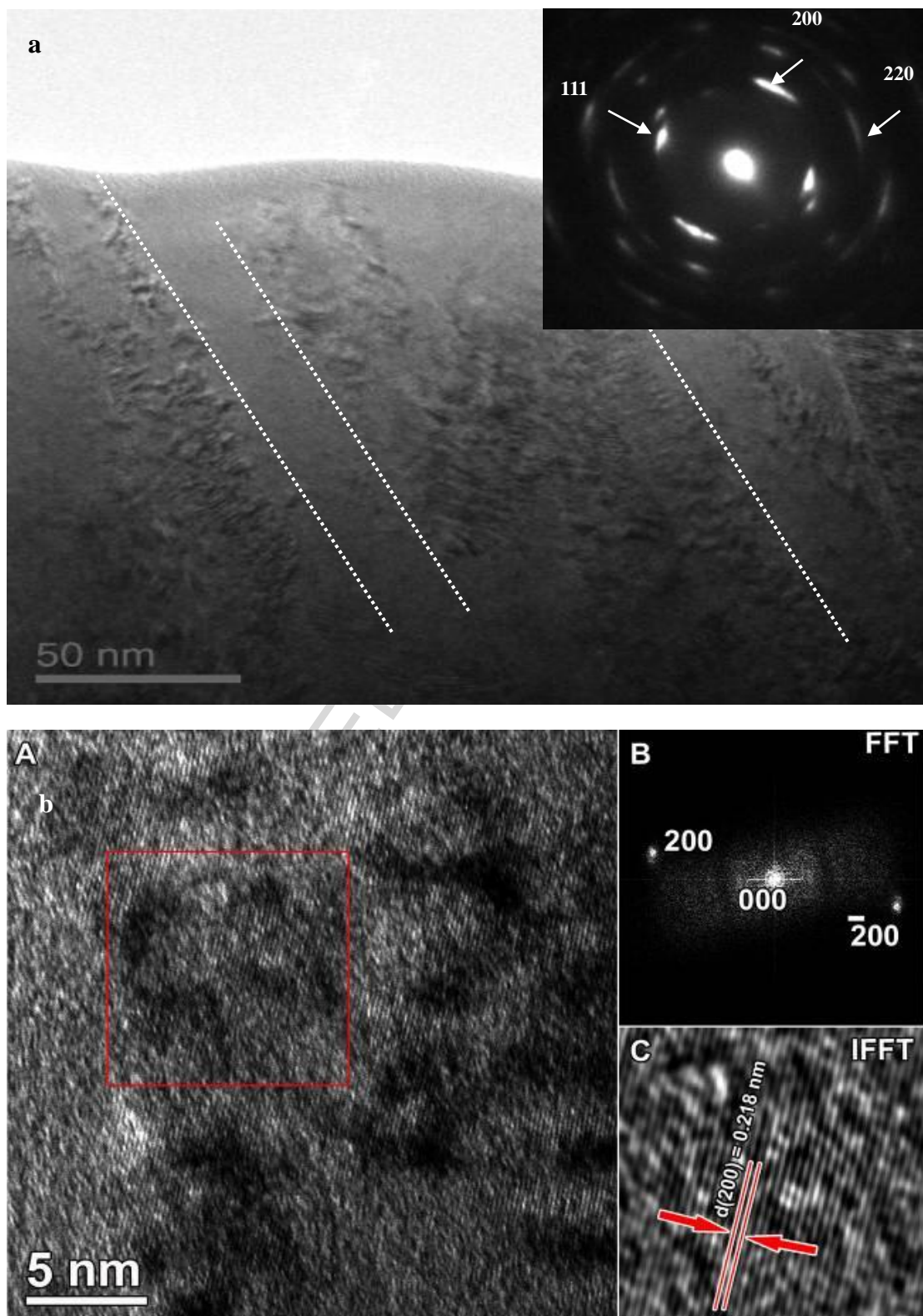
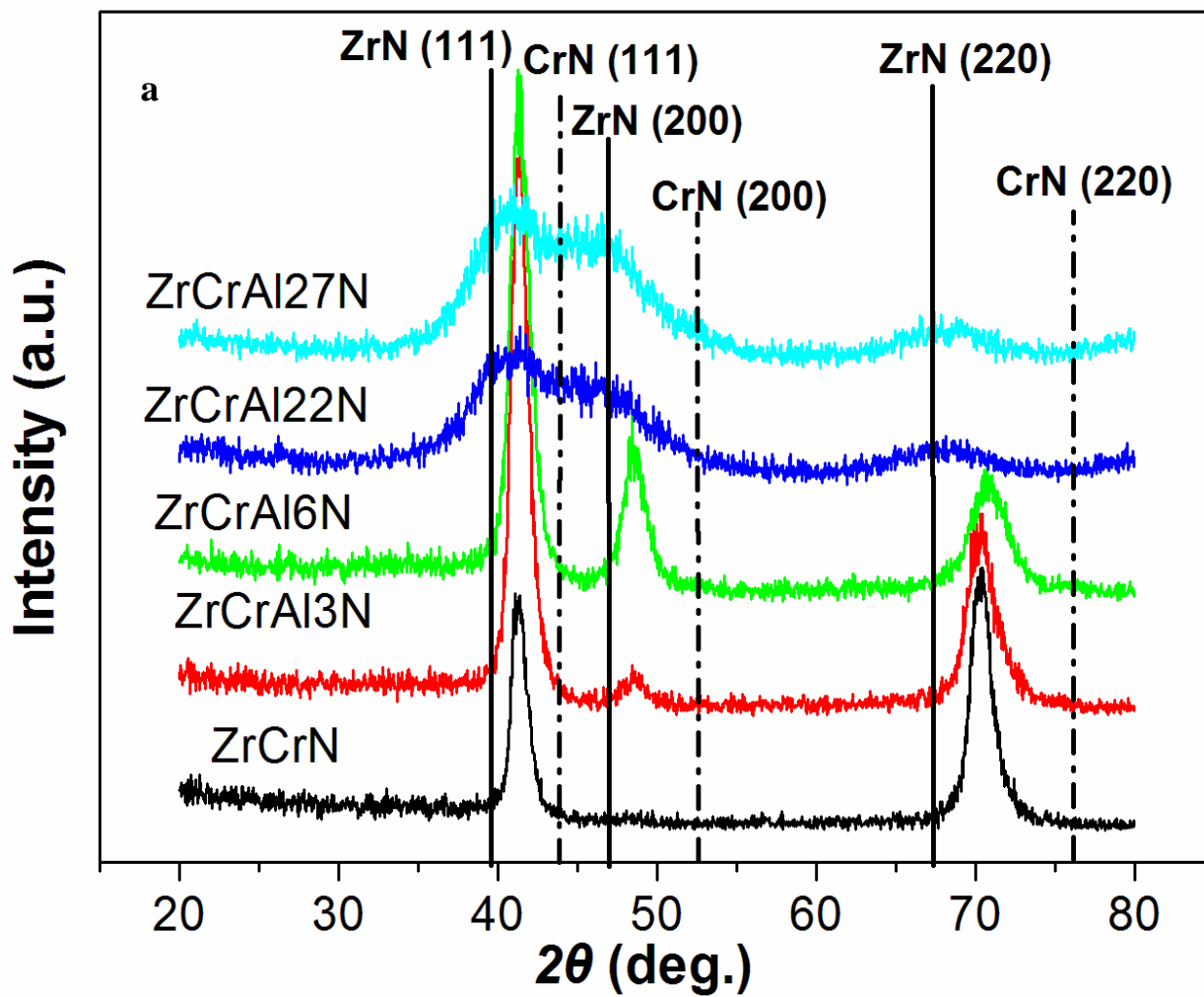
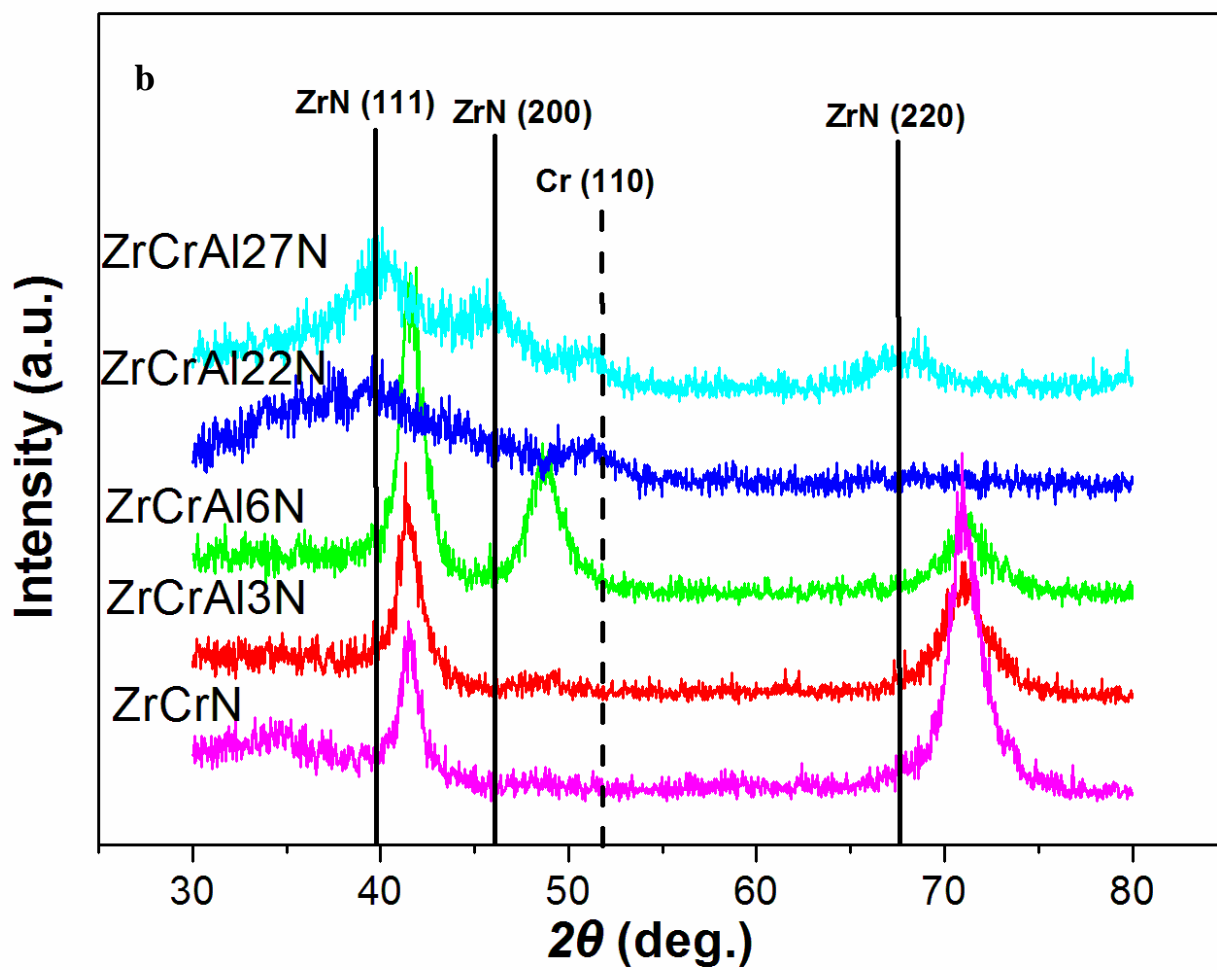


Fig.1 Cross-section BF-TEM (a) and typical HRTEM image (b) of the as-deposited ZrCrAl_3N coating. The corresponding SAD patterns are inserted in (a). The FFT spectra and IFFT image of the selected zone in (b) are attached in B and C, respectively.





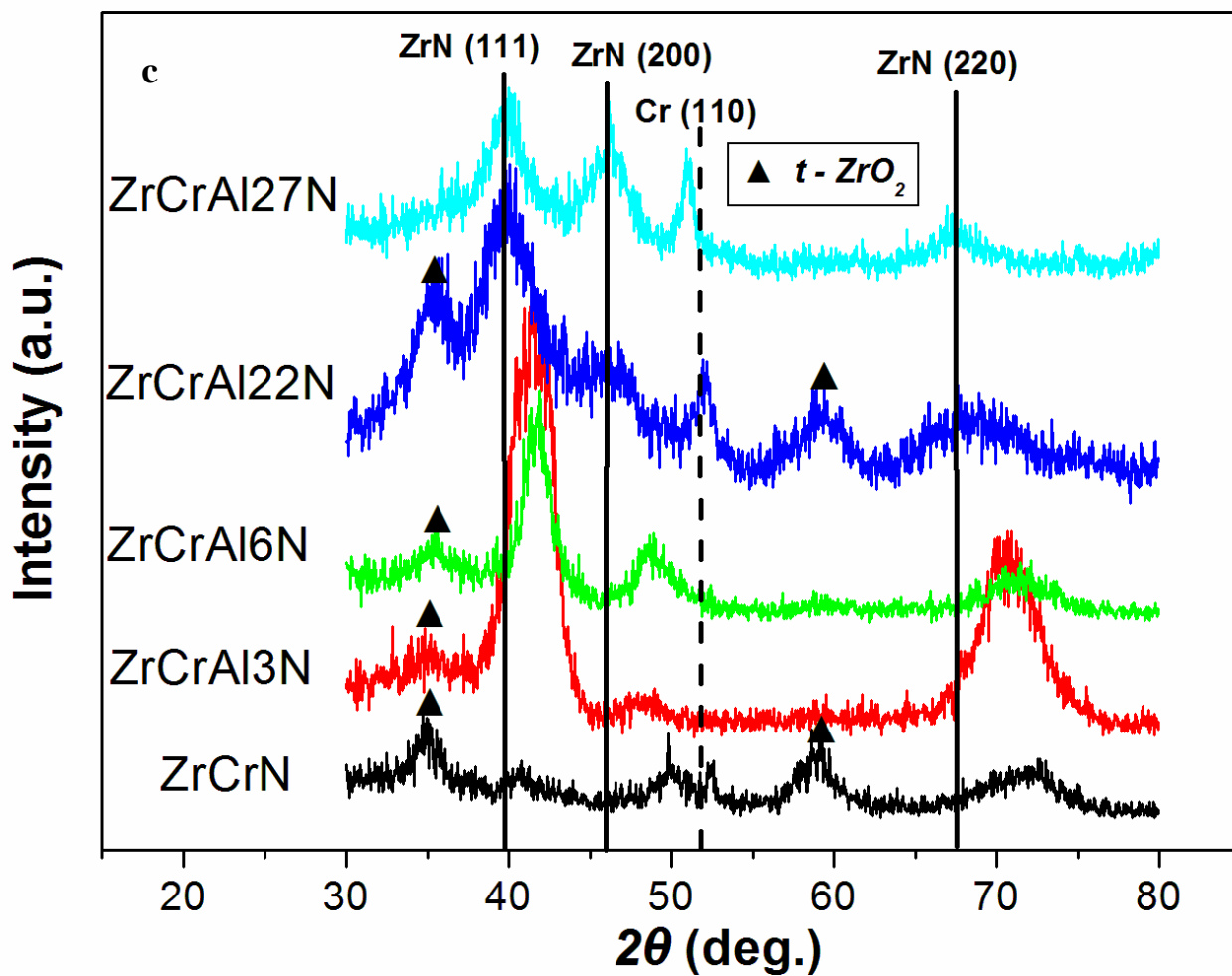
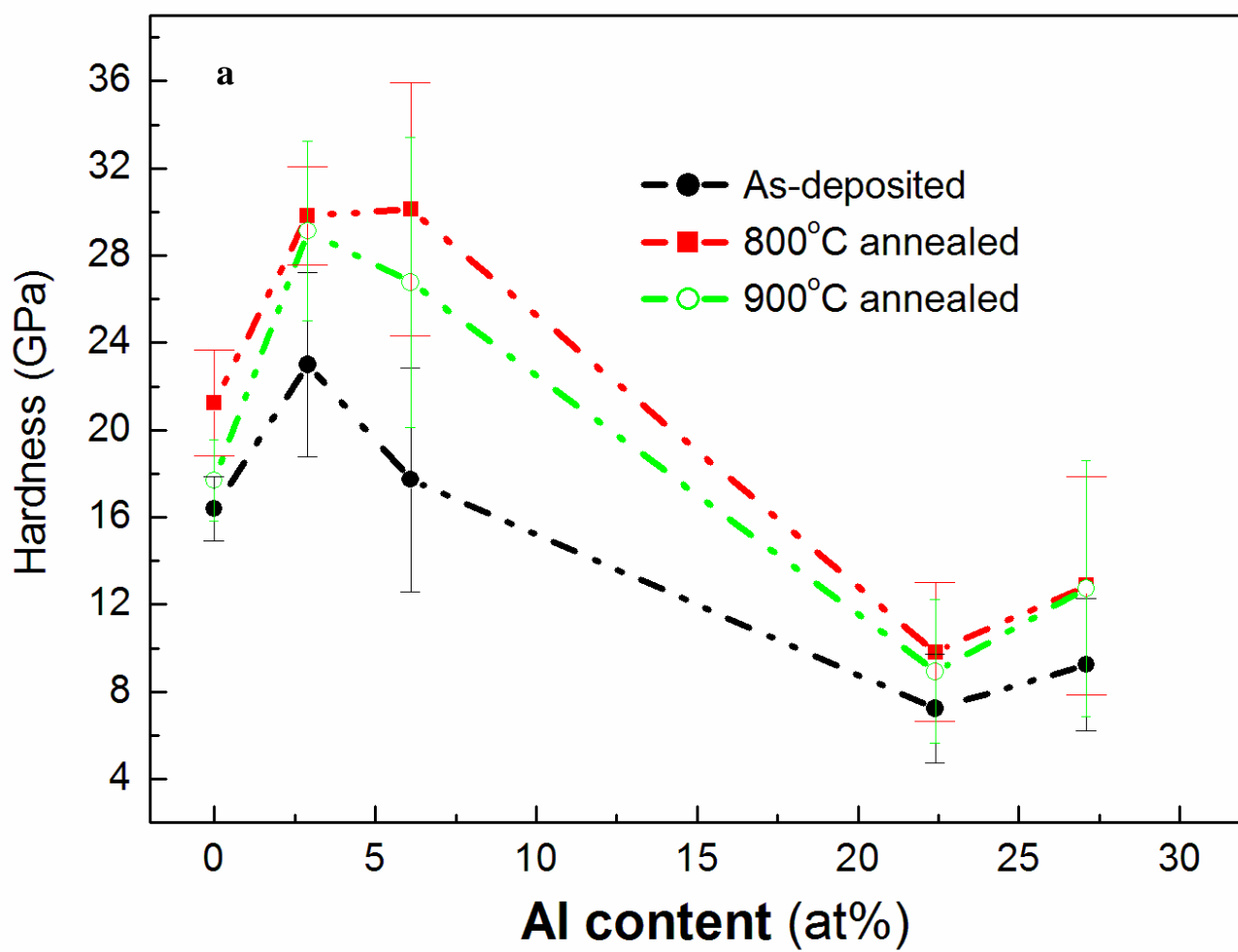
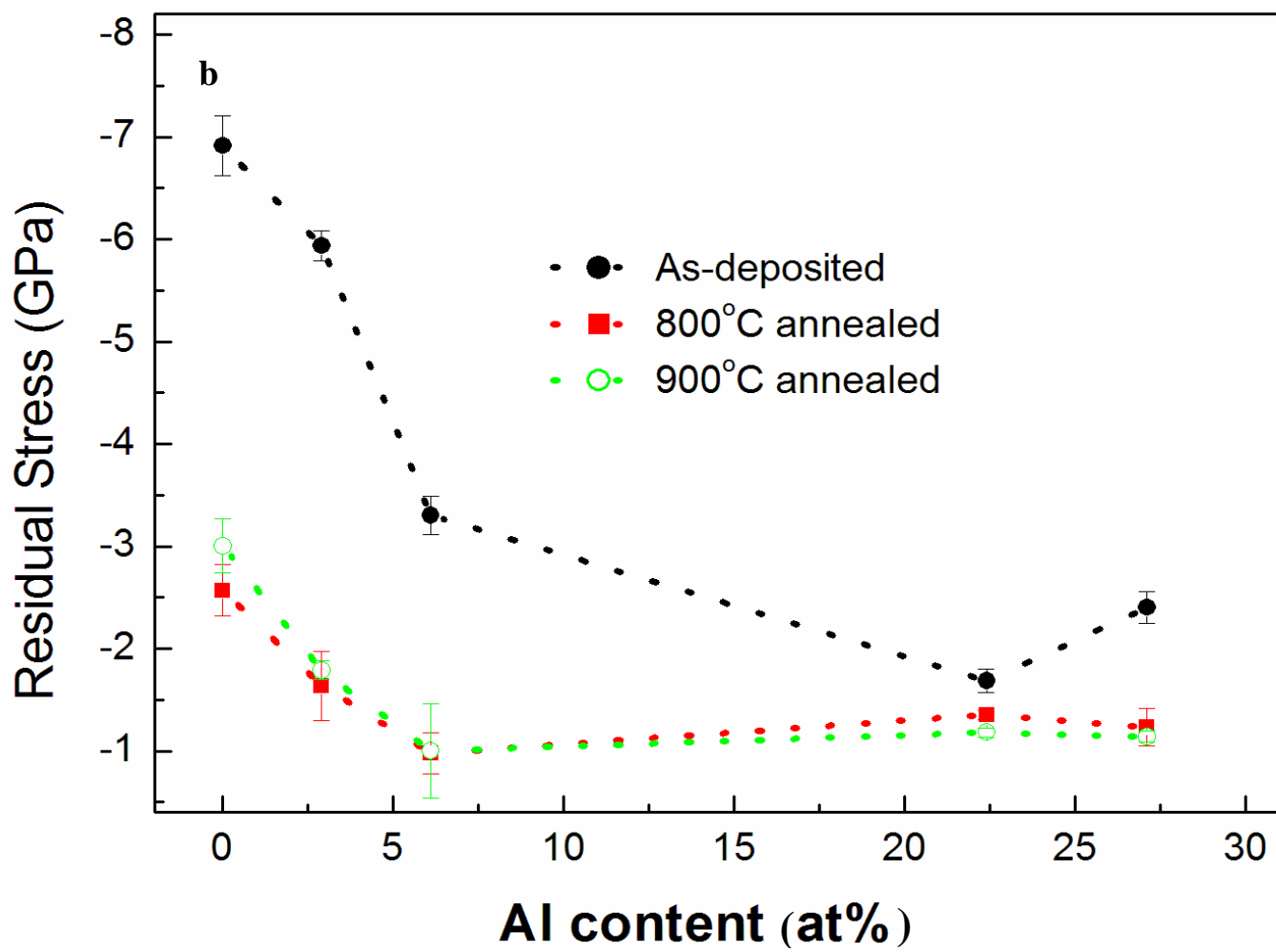
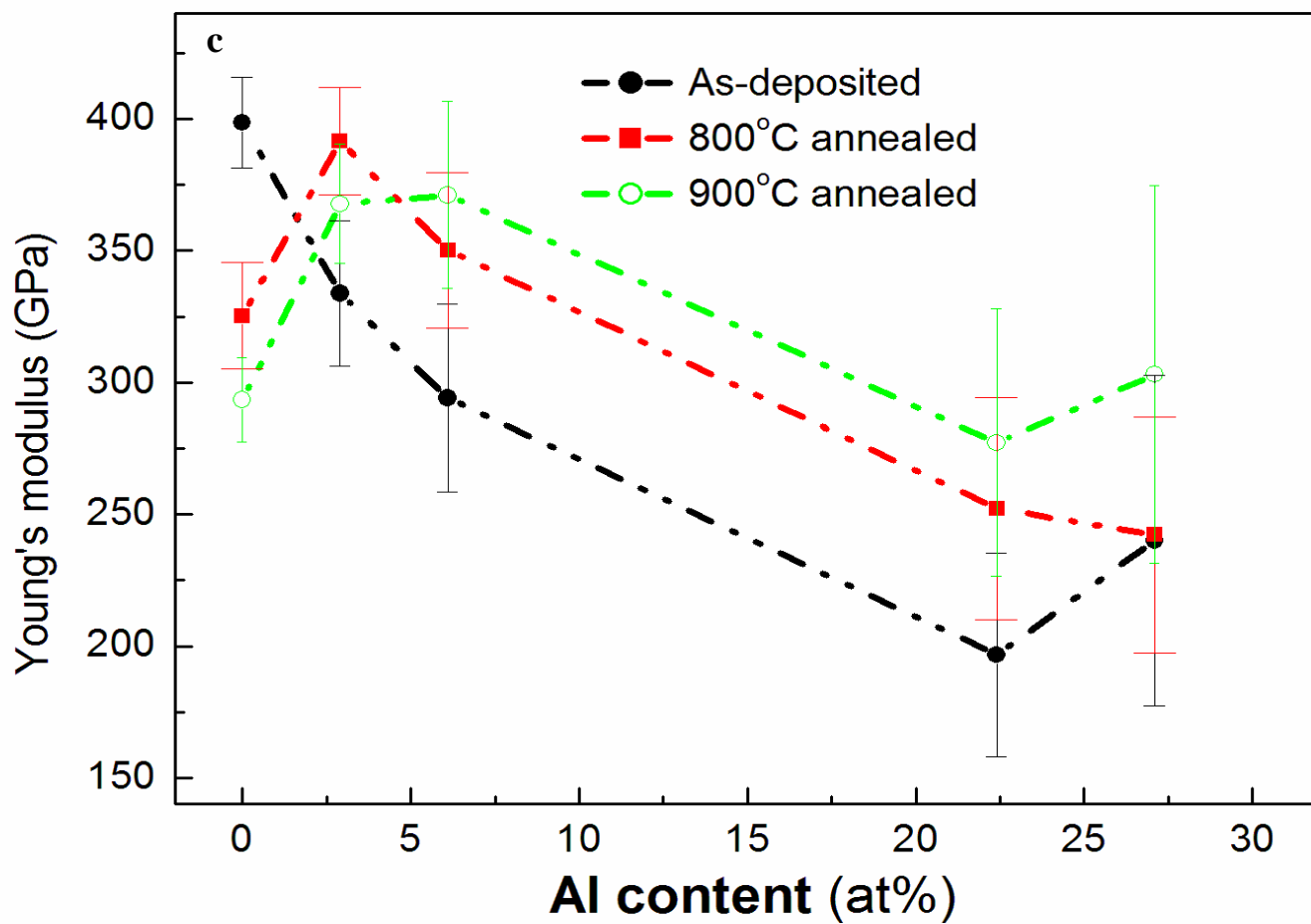


Fig.2 XRD patterns of the coatings as-deposited (a), annealed at 800 °C (b) and 900 °C (c).







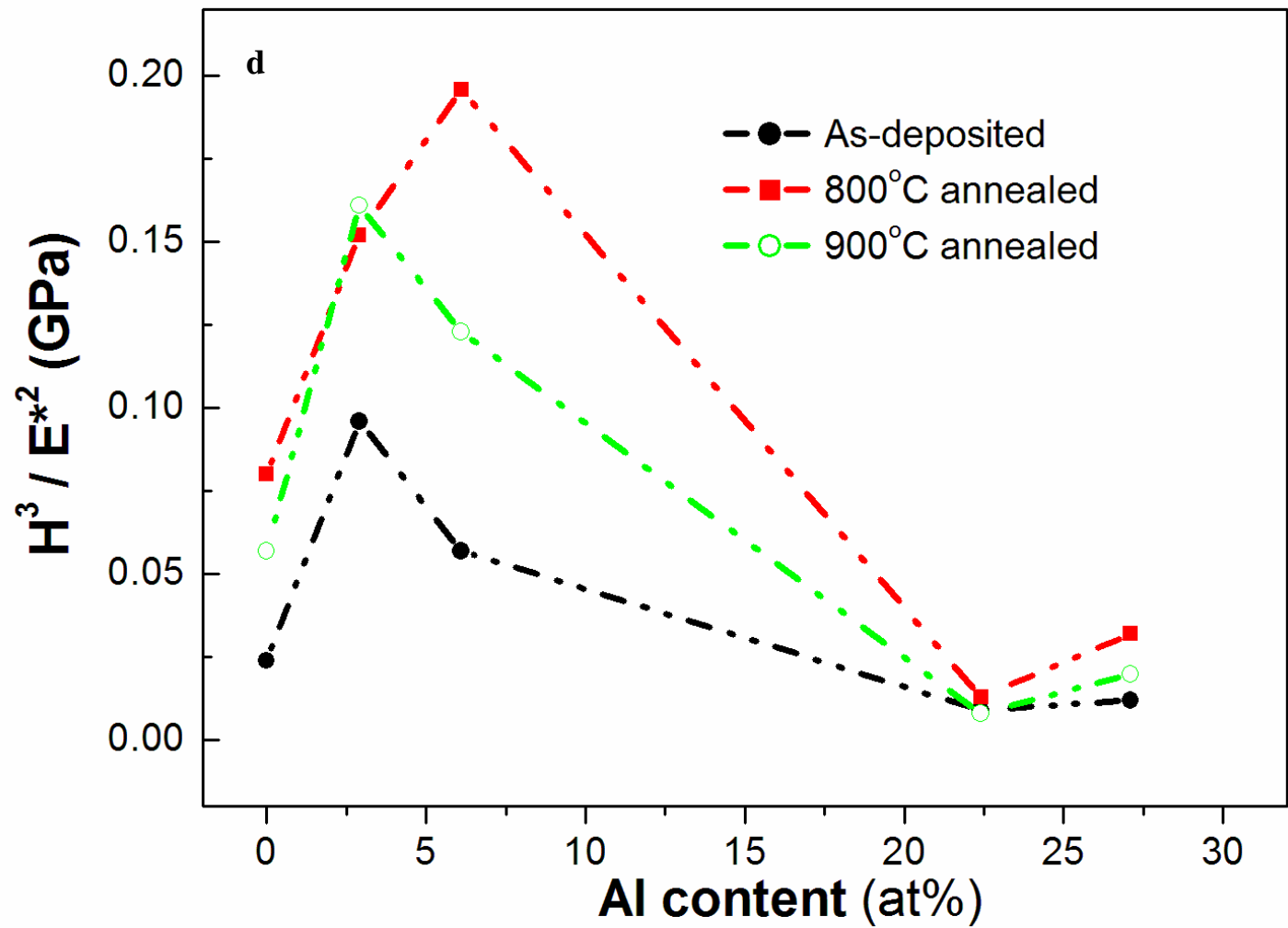


Fig.3. Hardness (a), residual stress (b), Young's modulus (c) and H^3/E^{*2} (d) of the as-deposited and annealed coatings.

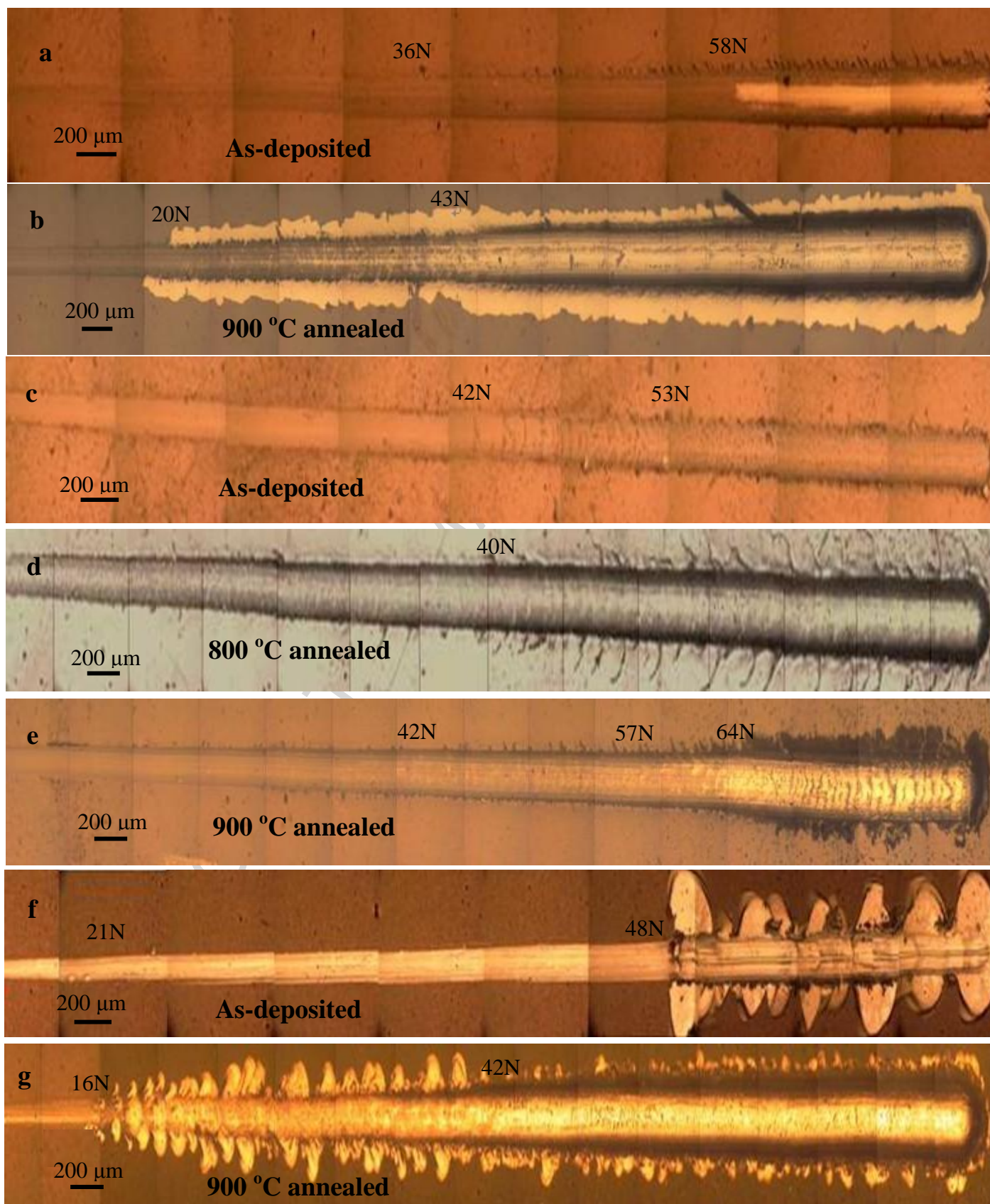


Fig.4. Typical track morphologies of the ZrCrN (a, b), ZrCrAl₃N (c, d, e) and ZrCrAl₂₇N (f, g) coatings before and after annealing.

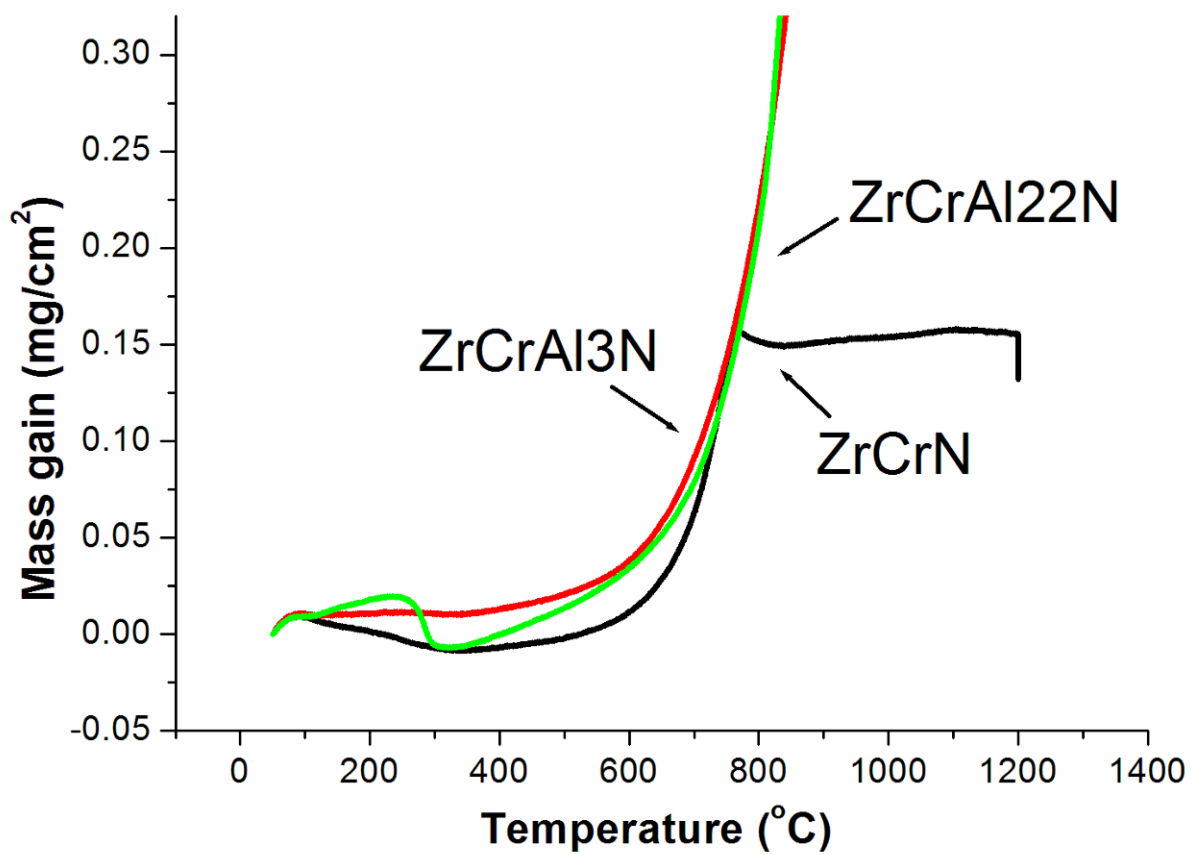
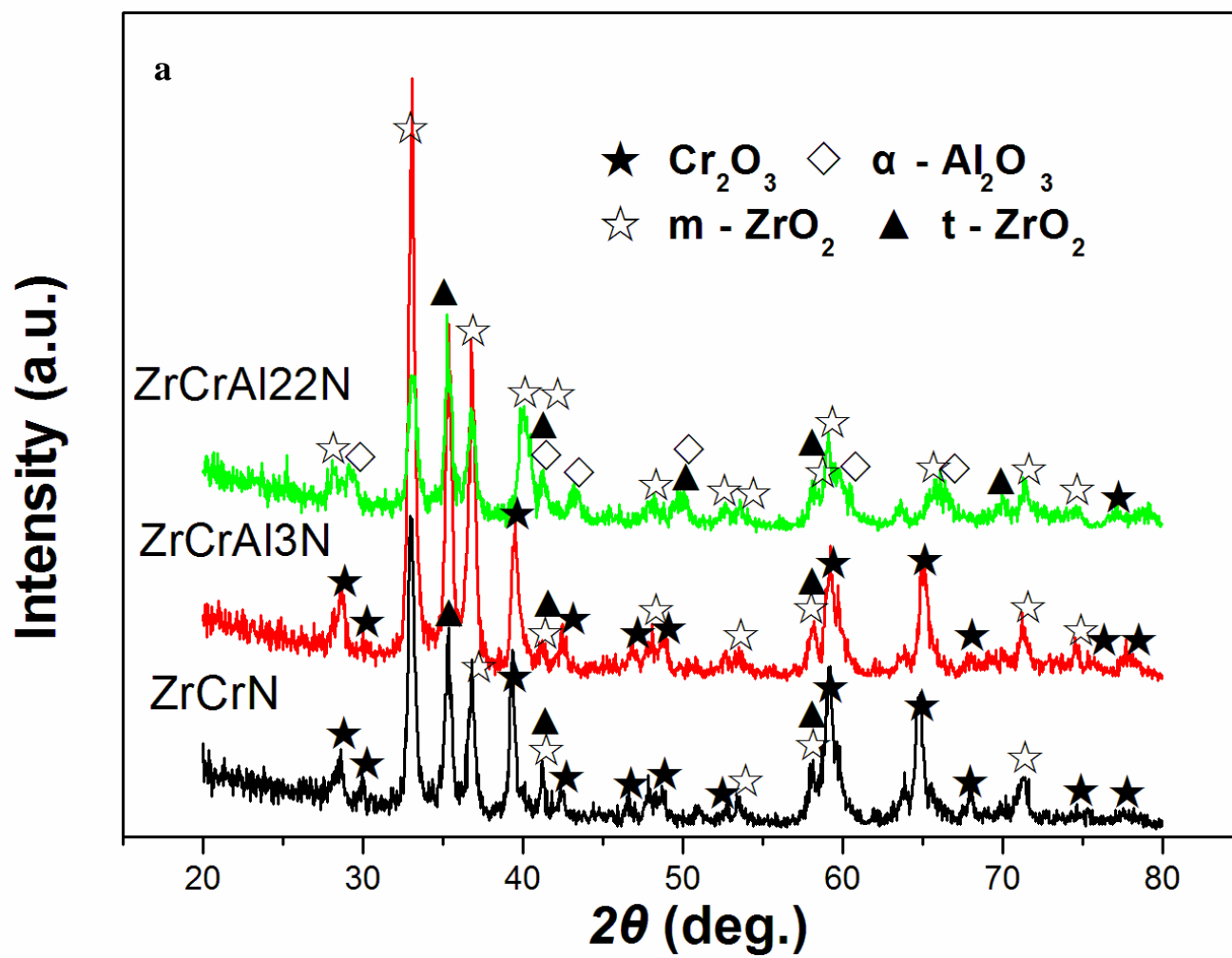
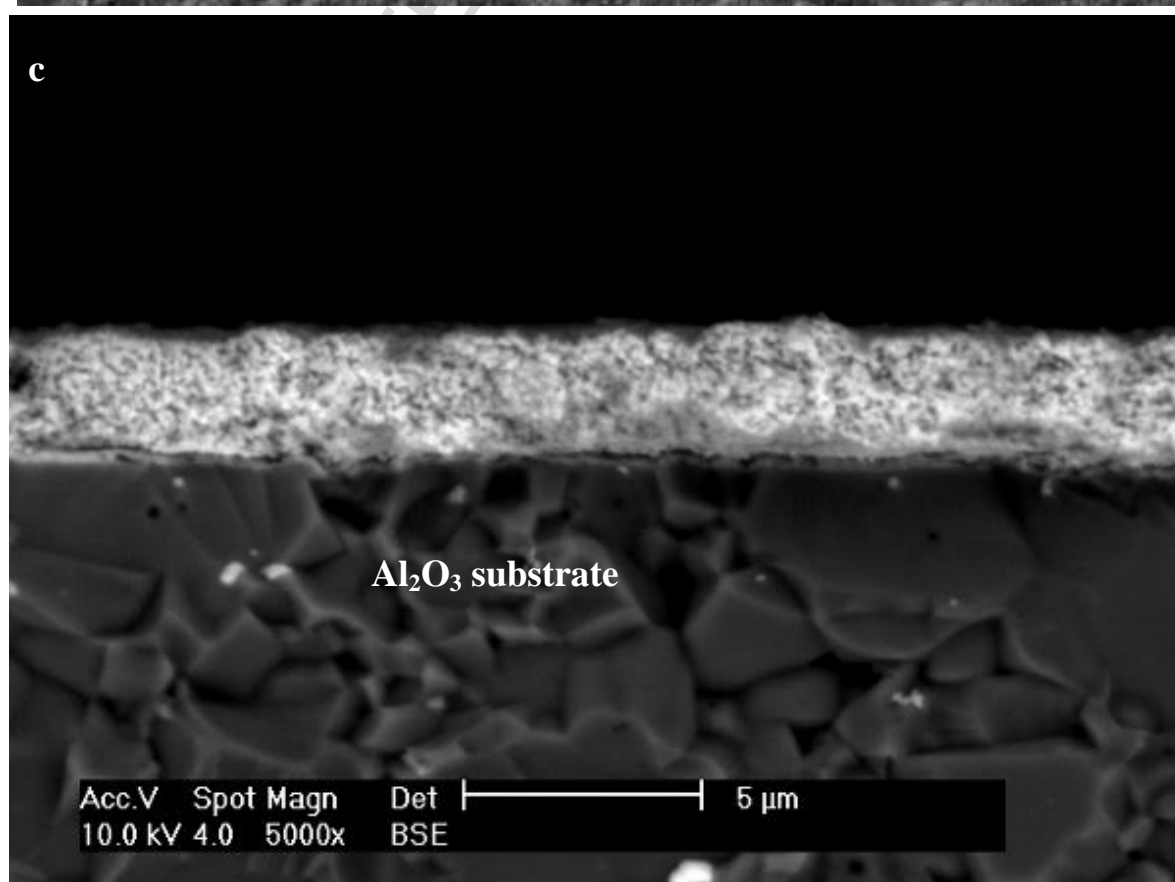
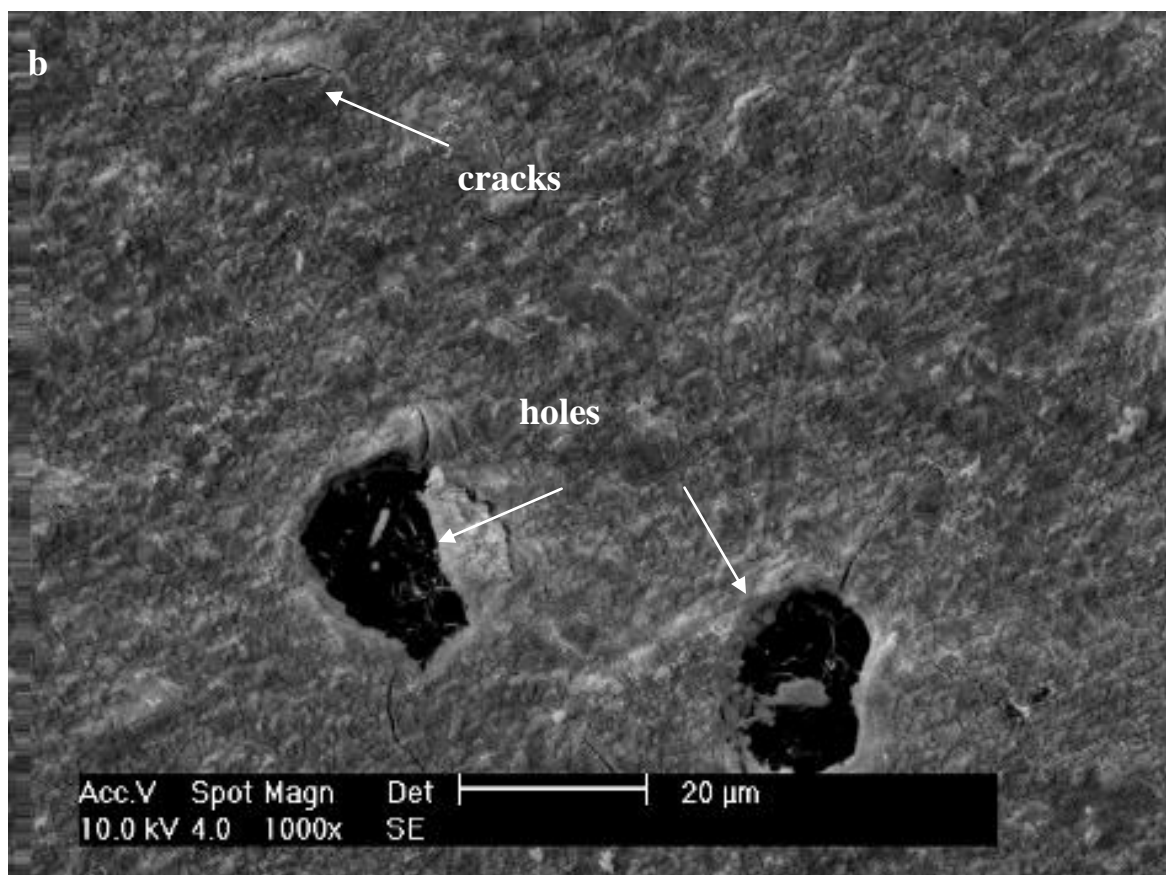


Fig.5. TGA curves of the ZrCrN, ZrCrAl₃N and ZrCrAl₂₂N coatings exposed to air from room temperature to 1200 °C.





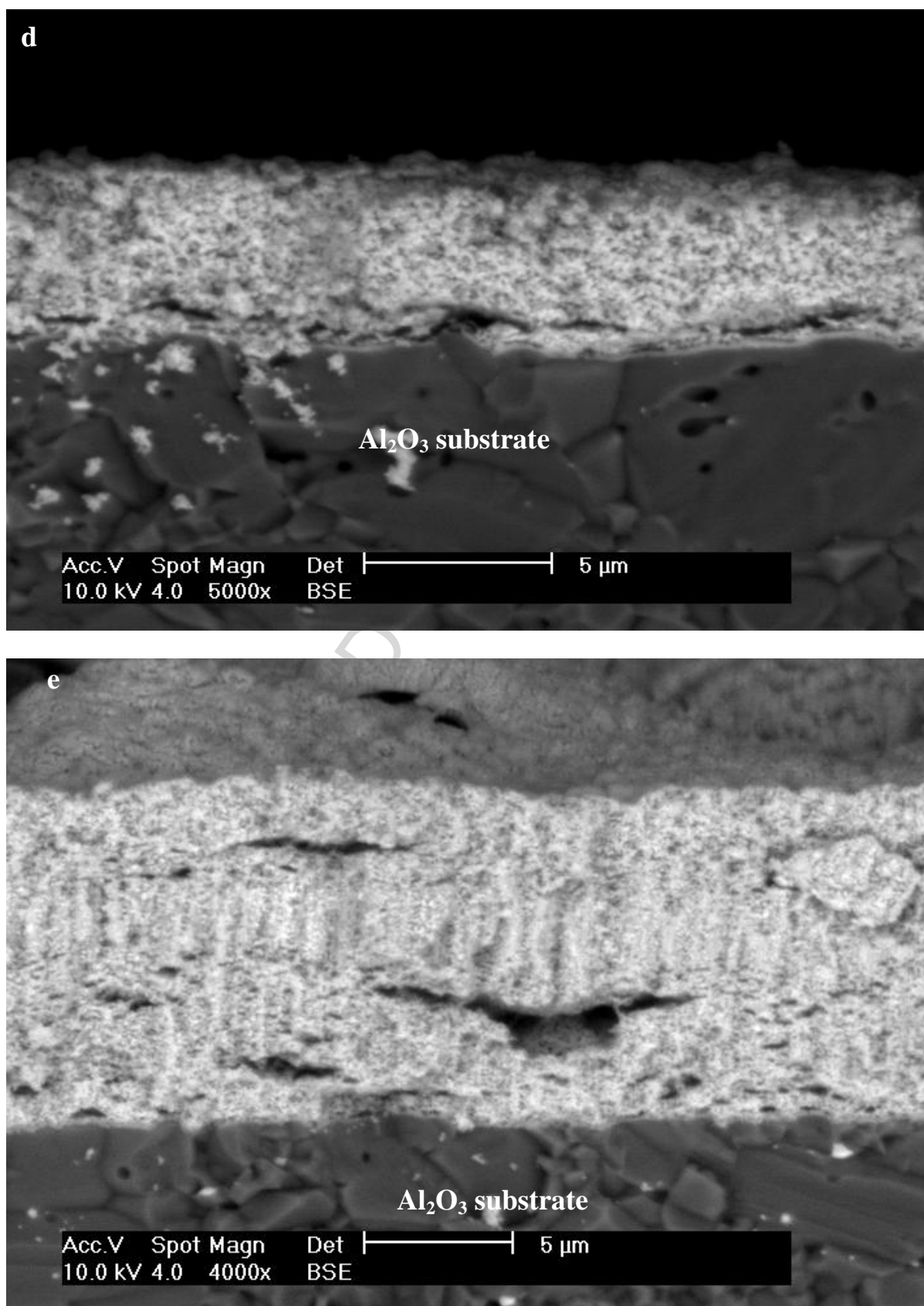


Fig.6. XRD patterns (a) and SEM images of the ZrCrN (b, c), ZrCrAl₃N (d) and ZrCrAl₂₂N (e) coatings exposed to air at 1200 °C for 1h.

Table 1 Chemical composition (by EDX), thickness and designated name of the coatings deposited at different Al target power densities (Cr target was set as 2.3 W/cm², Zr target as 6.0 W/cm²)

Al Target Power Density (W/cm ²)	Chemical composition (at.%)*				Designated name	Thickness (μm)
	Zr	Cr	Al	N		
0	25	25	0	50	ZrCrN	2.2
0.8	24	25	3	48	ZrCrAl3N	2.4
1.5	23	23	6	48	ZrCrAl6N	4.2
2.3	27	19	22	32	ZrCrAl22N	8.2
3.0	25	18	27	30	ZrCrAl27N	8.8

* All values $\pm 1\%$.

Highlights

Zr-Cr-Al-N coatings with low Al content exhibit high thermal stability.

Coating hardness and Young's modulus are enhanced after 800 or 900°C annealing.

Substrate softening affects the coating adhesive/cohesive strength.

The Zr-Cr-Al-N coatings start to oxidize at 600 °C.

ACCEPTED MANUSCRIPT